Highly dispersed $NbOPO_4$/SBA-15 as a versatile acid catalyst upon production of renewable jet-fuel from bio-based furanics via hydroxyalkylation-alkylation (HAA) and hydrodeoxygenation (HDO) reactions

Samikannu, Ajaikumar; Konwar, Lakhya Jyoti; Rajendran, Kishore; Lee, Cheng Choo; Shchukarev, Andrey; Virtanen, Pasi; Mikkola, Jyri Pekka

Published in:
Applied Catalysis B: Environmental

DOI:
10.1016/j.apcatb.2020.118987

Published: 05/09/2020

Document Version
Accepted author manuscript

Document License
CC BY-NC-ND

Highly Dispersed $NbOPO_4$/SBA-15 as a Versatile Acid Catalyst ~~for the~~upon Production of Jet-fuel from Bio-based Furanics via Hydroxyalkylation-Alkylation (HAA) and Hydrodeoxygenation (HDO) Reactions

Ajaikumar Samikannu[a,], Lakhya Jyoti Konwar[a], Kishore Rajendran[b], Cheng Choo Lee[a], Andrey Shchukarev[a], Pasi Virtanen[c] and Jyri-Pekka Mikkola[a,c,*]*

[a]Technical Chemistry, Department of Chemistry, Chemical-Biological Centre, Umeå University, SE-901 87 Umeå, Sweden

[b]Department of Chemical Engineering, Norwegian University of Science and Technology, Høgskoleringen 5, 7491 Trondheim, Norway

[c]Laboratory of Industrial Chemistry and Reaction Engineering, Johan Gadolin Process Chemistry Centre, Åbo Akademi University, Turku, FI-20500, Finland

*Corresponding Author: ajaikumar.samikannu@umu.se; ~~jyri-pekka.mikkola@umu.se~~

ABSTRACT

Herein, we report the preparation of highly dispersed and active Brönsted acidic $NbOPO_4$ (NbP) loaded mesoporous SBA-15 catalysts by means of a simple deposition method. The as prepared NbP/SBA-15 catalysts were thoroughly characterised by means of different techniques such as XRD, FT-IR, XPS, NH_3-TPD, SEM-EDX, TEM, TGA, ^{31}P-MAS-NMR and N_2-physisorption measurements. The deposition method was found to be effective for obtaining high surface area catalytic materials without altering the structure and surface properties of SBA-15. These materials overcome the drawbacks of Al-SBA-15, ZSM-5, bulk $NbOPO_4$ catalysts and demonstrated high catalytic activity upon the synthesis of jet-fuel range hydrocarbons precursors via hydroxyalkylation-alkylation (HAA) of bio-based carbonyl compounds with 2-methyl furan (carbonyl conversion upto ~100% and ≥93 % HAA product selectivity in 5h at 40-60 °C under solventless conditions). The characterization results revealed that the structural

Formatted: English (United States)
Formatted: English (United States)
Formatted: English (United States)
Formatted: English (United States)
Formatted: English (United States)
Formatted: English (United States)
Formatted: English (United States)
Formatted: English (United States)
Formatted: English (United States)
Formatted: English (United States)
Formatted: English (United States)
Formatted: English (India)
Field Code Changed
Formatted: English (India)
Formatted: English (India)
Field Code Changed
Formatted: English (India)
Formatted: English (India)
Formatted: English (India)
Formatted: English (India)
Formatted: English (United States)
Formatted: Font: 12 pt, English (United States)
Formatted: English (United States)
Formatted: Default Paragraph Font, Font: Calibri, 11 pt, English (United States)
Formatted: Default Paragraph Font, English (United States)
Formatted: English (United States)
Field Code Changed
Formatted: English (United States)
Formatted: English (United States)
Formatted: English (United States)
Formatted: English (United States)
Formatted: English (United States)

features of the support and the supported catalysts remained stable, the catalysts were reusable several times and robust in terms of converting bio-based molecules into jet-fuel range precursors. Furthermore, the 5% Pd loaded NbP-B/SBA-15 catalysts showed superior activity and selectivity upon subsequent hydrodeoxygenation of HAA products into jet-fuel range hydrocarbons outperforming the commercial Pd/carbon catalysts. HAA conversion of about 100% was received at a low temperature (200 ºC) and 50 bar H_2 pressure and consistent with 100 % C9-C16 branched hydrocarbons selectivity.

KEYWORDS: Supported solid acid catalysts; niobium oxyphosphate; hydroxyalkylation-alkylation; hydrodeoxygenation; jet-fuel hydrocarbons

Formatted: English (United States)

1. INTRODUCTION

The depletion of crude oil reservoirs, the increasing energy demand and the stricter environmental regulations concerning the use of fossil fuels are stressing the energy sector and the transportation fuel industries to find alternative renewable fuels[1-2]. First generation biofuels were under intensive investigation during the last decade but, however, the use of food crops to produce biodiesel was highly debated and, at the same time, the use of expensive raw materials was economically not feasible and unrealistic in the long-term perspective[3]. Apart from the fuel cost, first generation fuels (alcohols, ketones and esters) contain oxygen, possess low energy density and are less competitive than the crude petroleum-based fuels[4-5]. In the recent years, renewable fuels (second generation biofuels) from non-food biomass materials received much attention and are considered to be a potential alternative to fossils and could diminish the dependency of fossil fuels in future. Second generation biofuels are to a large extent derived from forestry biomass residues (lignocellulose, cellulose), agricultural wastes, and household wastes through enzymatic or catalytic valorization of cellulosic carbohydrates into bioethanol, biobutanol and C4-C6 platform chemicals and, further catalytically converted into fuel-range

hydrocarbons[6]. Furanics such as furfural, hydroxy methylfurfural, 2-methyl furan, butanaldehyde, and cyclohexanone are the potential feed stock molecules derived from lignocellulose that can be catalytically converted in to high density jet-fuel range hydrocarbons (C9 to C16) via hydroxyalkylation/alkylation (HAA), followed by hydrodeoxygenation (HDO) reactions[7-10] as shown in Scheme 1. Several researchers studied this reaction mostly applying a two-step process using both homogeneous and heterogeneous catalysts. The first step hydroxyalkylation/alkylation (HAA) of 2MF with ketones or aldehydes were studied using formic acid, acetic acid, supported acidic ionic liquids, HCL, H_2SO_4, H_3PO_4, p-toluene sulphonic acids, zeolites, alumino silicates, metal phosphates, metal oxides and polymer resin catalysts etc.[11-15]. The second step hydrodeoxygenation of obtained HAA were studied over Pd/C, Pt/C Ni/ZrO_2-SiO_2, Cu,Pt/SiO_2, Ni/Hβ, Ni/ZSM-5 and Pd/$NbOPO_4$ catalysts[16-19] .

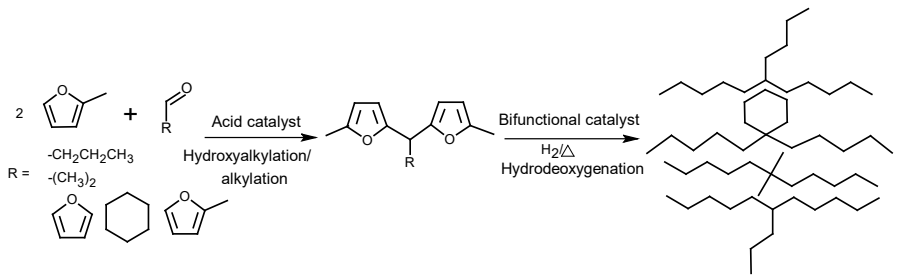

Scheme 1. Reaction pathways for obtaining fuel range hydrocarbons from biomass derived aldehyde, ketones and furanics.

The hydroxyalkylation/alkylation (HAA) reaction required strong Brönsted acid catalysts, as such the conventional mineral acids (HCl, H_2SO_4 and H_3PO_4) exhibit highest catalytic activity, however, their use causes serious disadvantages such as equipment corrosion, poor product selectivity due to side reactions, more waste generation causing pollution, handling and separation difficulties etc., Zeotype materials finds potential alternative to homogeneous acid

catalysts in many industrial applications but its microporous nature as well as lack of strong Brönsted acidity limits their use in HAA reaction. Finding new solid acid catalysts as well fine tuning the surface properties of the existing solid acid catalysts to achieve higher activity and selectivity has received much attention because of their potential use in industrial practices. Obtaining mesoporous solid acid catalyst with enough acid strength and operational stability is challenging and the quest of serving green catalyst in reactions involving bulkier molecules is still being actively pursued. Recently, niobium-based catalysts such as niobic acid (Nb_2O_5) and niobium phosphate ($NbOPO_4$) were extensively studied in acid catalyzed reactions because of their unique properties such as their thermal stability, acid strength and water tolerable properties[19-21]. Crystalline niobic acid and $NbOPO_4$ possess very low surface areas (<12 m^2/g)[22] and, also niobium is an expensive metal and its limited availability on earth limits its use in industrial applications. Several researchers attempted to increase its surface area in order to increase the number of available acid sites either by trying to make the material porous and amorphous or disperse it over porous carriers[23-26]. Zhang *et al*., prepared mesoporous $NbOPO_4$ in the presence of cetyltrimethylammonium ammonium bromide (CTAB) with varying p^H conditions and obtained porous amorphous material with maximum surface area of 290.1 m^2/g[27] Mal *et al*., used a supramolecular templating mechanism and used different templates thus obtaining a porous niobium phosphate with a maximum surface area of 482m^2/g[28-29]. Very few reports are available that report the dispersion of $NbOPO_4$ over mesoporous silica carriers since the use of phosphoric acid in the preparation step causes severe impacts on the surface properties of the support[30]. Francisco *et al*., dispersed $NbOPO_4$ over SiO_2 via a two-step synthesis procedure and obtained a good dispersion of NbP over SiO_2. Li-wei *et al*., prepared NbP-SBA-15 catalysts by treating Nb containing SBA-15 with diluted phosphoric acid that demonstrated a superior activity upon dehydration of fructose to 5-HMF[31]. However, the lack

of characterization details renders it hard for the readers to understand the properties of the studied materials.

In the present work, we utilize the structural uniqueness of SBA-15 material[32,33] (high surface area ≥ 900 m^2/g, large pore size and pore wall thickness ~5-7 nm, pore volume ≥1.0 cm^3/g) and report an effective protocol to disperse $NbOPO_4$ (NbP) over the mesoporous SBA-15 carrier preserving its surface and structural properties. Most importantly the immobilization/deposition could be achieved under mild temperatures (ambient to 80 °C) in a simple preparation method utilizing non-corrosive and non-toxic $NH_3H_2PO_4$ as phosphorous precursor in contrast to the reported literature by other researchers using concentrated H_3PO_4.[30-31] All the NbP/SBA-15 catalysts prepared using different synthesis conditions were thoroughly characterized by various physico-chemical characterization techniques (XRD, FT-IR, XPS, NH_3-TPD, SEM-EDX, TEM, TGA, ^{31}P-MAS-NMR and B.E.T nitrogen measurements) to understand better the correlation between the structural properties with their efficiency in catalytic reactions. The catalytic activity of the as prepared NbP/SBA-15 catalysts were subsequently explored on the production of renewable jet-fuel and diesel range hydrocarbons via a two-step hydroxyalkylation-alkylation (HAA) of the bio-based aldehydes and ketones with 2-methyl furan (step I) and subsequent hydrodeoxygenation of the HAA products (step II) over 5% of Pd containing the NbP/SBA-15 catalysts.

2. EXPERIMENTAL

2.1. Materials and methods

Tetraethyl orthosilicate and Pluronic 123 (poly-(ethylene glycol)-block-poly(propylene glycol)-block poly(ethylene glycol)-copolymer, EO_{20}-PO_{20}-EO_{20}, M_n ~5,800), niobium (V) chloride (99%), aluminium isopropoxide(≥98%), $Pd(NO_3).xH_2O$, 2-methylfuran (99%), 1-butanal (99.5%), furfural (99%) were received from Sigma-Aldrich. Acetone (99.9%),

Formatted: English (United States)

Formatted: English (India)

acetonitrile (99.9%), ethanol (99.9%), HCl (37%), were received from VWR International. Ammonium dihydrogenphosphate (99%) from Merck, cyclohexane (99.7%) and dicholoromethane (99.99%) were received from Fisher chemicals. Commercial catalysts such as 5wt.%Pd/carbon was purchased from Sigma-Aldrich and H-ZSM-5 (SiO_2/Al_2O_3=23) from Zeolyst international. All the chemicals used as received from the suppliers without further purification.

2.2. Catalyst preparation

2.2.1. Synthesis of Si-SBA-15 and Al-SBA-15

The mesoporous silica SBA-15 and Al-SBA-15 with Si/Al ratio of 25 were synthesized according to the reported literature procedures[32,33]. In a typical synthesis protocol, 20 g of the structure directing agent, triblock copolymer (poly(ethylene oxide)-poly(propylene oxide)-poly (ethylene oxide) and Pluronic 123 were dissolved in a polypropylene bottle using 600 mL of a 1.5M HCl solution and stirred constantly at 40 ºC for 3 h. The second solution was prepared by dissolving 42.5g of silica source, tetraethyl orthosilicate (TEOS), in a 150 mL of 1.5M HCl solution and then added slowly to the first solution. Stirring was continued for 24 h and then the resulting gel was aged at 95 ºC for 48h under static conditions. In the case of Al-SBA-15, the calculated amount of aluminium isopropoxide was introduced to the second solution to obtain a Si/Al ratio of 25. After aging, the resultant solid product was filtered, washed thoroughly with deionized water to reach neutral pH, dried overnight at 100 ºC in an oven and finally, the organic template in the as synthesized material was removed by calcination in flowing air at 550 ºC for 6 h.

2.2.2. Preparation of NbP and Nb_2O_5 containing SBA-15 materials

Niobium oxyphosphate (NbP) was supported on Si-SBA-15 material by means of different preparation conditions varying different HCl concentrations. In a typical preparation method, the pre-dried Si-SBA-15 was suspended in deionised water and stirred using a magnetic stirrer. Then, the required amount of niobium chloride precursor was hydrolysed in deionized water and added slowly to the above slurry to achieve 10 wt.% of Nb on SBA-15 and the mixture was stirred at 80 ºC. After this, the required/stoichiometric amount of ammonium dihydrogen phosphate (a slight excess in terms of the concentration of Nb) was dissolved in deionized water, added to the above mixture and stirred for 5h. The resultant material was filtered, washed thoroughly with deionised water, dried overnight at 100 ºC and finally calcined at 400 ºC for 5 h, hereafter, the catalyst was denoted as NbP-A/SBA-15. A similar procedure was used to prepare the NbP-B/SBA-15 catalyst using a 1M HCl solution. Similarly, NbP-C/SBA-15 and NbP-D/SBA-15 catalysts were prepared using 37%HCl solutions, the former at 80 ºC and the latter at room temperature, respectively. Bulk NbP was also prepared using the conditions similar to that used upon preparation of the NbP-C/SBA-15 and, thereafter, the catalyst was denoted as the NbP-bulk. 10wt.% of Nb_2O_5 containing SBA-15 catalyst was also prepared by means of a wet-impregnation method using ethanolic solutions. In a typical preparation, 1 g of the pre-dried Si-SBA-15 was dispersed in 20 mL of 99.5% ethanol solutions, the calculated amount of $NbCl_5$ to obtain 10wt.% Nb_2O_5 was dissolved in 5mL of 99.5% ethanol which was slowly added to the above slurry under constant stirring. As the next step, 5 mL of 10 vol.% ethanol-water solution (99.5% ethanol: water) was slowly added and stirred further for 8h, the solvent was removed by a rotary evaporation and the resulting solid was dried overnight at 100 ºC and calcined at 550 ºC for 6 h.

2.2.3. Preparation of palladium containing NbP/SBA-15 materials.

The palladium containing NbP/SBA-15 material was prepared by means of the incipient wetness method using Pd $(NO_3)_2.xH_2O$ as the Pd precursor. Pd/NbP/SBA-15 was obtained by impregnating NbP/SBA-15 with a calculated amount of palladium nitrate precursor solutions in order of obtaining 5wt% of Pd. (the volume of the precursor solution was calculated to be equal to the pore volume of the support obtained by the B.E.T. isotherms). The impregnated sample was dried overnight at 100 ºC, calcined at 300 ºC for 3h (ramp 2 ºC/min under an air flow of 30mL/min) and further reduced at 300 ºC/3h (ramp 1 ºC/min under 10 mL/min of H_2 flow.

2.3. Material characterization.

All the as-prepared NbP/SBA-15 catalysts were extensively characterised by means of different physico-chemical techniques. Small and wide-angle powder X-ray diffraction patterns of the catalysts were recorded on a PANalytical diffractometer using Cu Kα (λ = 0.154 nm) radiation. The diffractograms were recorded in the 2θ range of 0.5–10º (small angle) and 10 to 70º (wide angle) in the steps of 0.025º with a count time of 15s, at each point. The infrared spectra were recorded using the Bruker Vertex 80v FT-IR spectrometer with vacuum bench and a DTGS detector. The MAS-NMR spectra were recorded using a Bruker Avance III 500 MHz spectrometer with 4 mm zirconia rotors spun at a magic angle of 10 kHz. The ^{31}P direct polarization (DP) MAS spectra (96 scans) were measured at room temperature using a ^{31}P π/2 pulse length of 7.3 μs and the TPPM proton decoupling sequence at 50 kHz. The relaxation delay was 400 s to allow for complete recovery of all the species in the spectra. The chemical state of the different species on the support were examined by means of the X-ray photoelectron spectroscopy. All the XPS spectra were recorded with a Kratos Axis Ultra electron spectrometer equipped with a delay line detector. A monochromated Al Kα source operated at 150 W, hybrid

lens system with magnetic lens, providing the analysis area of 0.3 x 0.7 mm^2, and charge neutralizer were used during all the measurements. The binding energy (BE) scale was referenced to the C1s line of aliphatic carbon, set at 285.0 eV. Further, the processing of the spectra was accomplished with the Kratos software. The textural and surface morphology of the catalytic materials were studied on a Carl Zeiss Merlin Field Emission Scanning Electron Microscope (FE-SEM) operating at a 30 kV equipped with an energy-dispersive X-ray spectroscopy (EDS, Oxford Instruments X-MAX 80 mm^2 X-ray Detector). The N_2 adsorption-desorption measurements were performed using a Micromeritics TriStar porosimeter, CiAB Chemical Instruments AB. The adsorption-desorption isotherms were recorded at 77 K after degassing the samples at 473 K for 3h. The surface areas were calculated by the B.E.T. method and the pore volumes were calculated from the corresponding desorption isotherms. The pore size distributions were estimated using the Barrett, Joyner and Halenda (BJH) algorithm (ASAP-2010) available as a built-in software from Micromeritics. Total acidity of the catalysts was determined by means of the temperature-programmed-desorption method (TPD) on a BELCAT II instrument (MicrotracBEL Corp.). For all acidity measurements, 5% NH_3 in helium was used as a probe molecule. In a typical measurement, about 50 mg of the sample was placed in an adsorption vessel and the sample was evacuated at 450 °C for 2 h under helium flow. Subsequently, the sample was cooled down to 50 °C, the catalyst was saturated with 5%NH_3 in helium for 1h and subsequently flushed with helium, at 100 ºC for 1h, to remove traces of physisorbed NH_3. The desorption of ammonia was carried out from 100 to 500 °C, at a heating rate of 10 °C/min under He flow. After each measurement, the amount of chemisorbed ammonia was determined form the calibration curve obtained from varying volumes of NH_3 in helium. The thermogravimetric analyses of the catalysts were carried out in a TGA thermoanalyser (Cahn D-200). The samples were heated in a chamber in which the temperature was controlled by an oven (Carbolite Furnaces). The temperature program was as follows: 10

ºC/min from room temperature to 750 ºC, ending with the final temperature inside the chamber being ~735 ºC in an argon atmosphere.

2.4. Reaction setup and catalytic experiments

2.4.1 Hydroxyalkylation/alkylation (HAA)

The hydroxyalkylation/alkylation of 2-methylfuran with different aldehydes and ketones were carried out in a 5 mL micro batch reactor equipped with a heating block maintained at the required temperatures (40-60 °C) and, all the reactions were carried out under solventless conditions. In a typical experiment, 50mg of catalyst, 5.63mmol of 2-methyl furan and 2.5mmol of the aldehyde or ketone was loaded in the reactor and stirred constantly, at required temperatures, for a specific period of time. After each experiment, the reactor was settled to cool down inside a refrigerator before sampling and centrifuged later to separate the catalyst. After this, 100 µL of the reaction mixture was removed, diluted 10 times with acetonitrile and analysed by means of gas chromatography GC-FID (Agilent 6890 N) equipped with an Agilent J&W HP-5 column (30 m length, 0.25 mm internal diameter, and 1 µm of film thickness) and helium was used as the carrier gas. The GC injection port and the detector temperature were set at 250 °C and the column temperature was ramped from 50 to 250 °C, at the rate of 5 °C/min. The conversion of the aldehyde or ketone as well as the HAA product quantification were calculated from the GC peak areas with the help of the calibration curves obtained with standard compounds (the corresponding HAA products were purified by vacuum distillation for obtaining calibration curves). The HAA products were also confirmed by GC-MS (Agilent technologies model 5579N) with a HP-5MS capillary column (30m length, 0.25 mm internal diameter, 0.25 µm film thickness). The isolated HAA products were also confirmed by ^{1}H-NMR spectroscopy on a Bruker 400 MHz Avance III spectrometer at 25.5 °C using $CDCl_3$ as a solvent. (ESI, Fig. S1 to S4).

2.4.2. Hydrodeoxygenation (HDO)

The various HAA products thus obtained from hydroxyalkylation/alkylation reaction were further converted via hydrodeoxygenation (HDO) over 5%Pd loaded NbP/SBA-15 catalysts to produce jet fuel-range branched hydrocarbons. All of the catalytic experiments were performed in batch mode using a stainless-steel autoclave with a capacity of ~14 mL, equipped with a pressure indicator, an emergency relief valve and a digital temperature controller. In a typical reaction, 100 mg catalyst, 2.5 mmol of the HAA product and 3 mL cyclohexane solvent were loaded into the autoclave. In the next step, the reactor was flushed several times with pure hydrogen (99.99%) and pressurized further to reach the desired H_2 pressure of 50 bar, the reaction mixture was heated to the required temperature (200-300 ^oC) for the reaction period of 4-12h. After the reaction, the reactor was cooled down to room temperature, the H_2 pressure was carefully released, 10 µL of the reaction product was diluted with dichloromethane and analysed by means of gas chromatography GC-FID (Agilent 6890 N) equipped with an Agilent J&W HP-5 column (30 m length, 0.25 mm internal diameter, and 1 µm of film thickness). The hydrocarbon products were identified by means of GC-MS equipped with the same column as used during the GC-FID analysis.

3. RESULTS AND DISCUSSION

3.1. Catalyst characterization results

3.1.1. XRD results

The small and wide-angle X-ray diffraction patterns of the support and NbP/SBA-15 catalysts prepared under different conditions were presented in Fig. 1a and Fig.1b and the structural parameters such as *d*-spacing, lattice constant (a_0) and pore wall thickness of the materials are summarized in Table 1. Fig.1a displays three distinct peaks around 2θ, 0.9°, 1.4° and 1.6°, thus

indicating 100, 110 and 200 plan reflections, respectively, conforming the formation of well-ordered hexagonal Si-SBA-15.[32] The peak position, judged from the intensity of these reflections, was not significantly affected upon loading/deposition of NbP under different concentrations of HCl solutions at 80 °C and only slightly decreased intensity of the peaks was observed. However, noticeable changes in the parameters such as *d*-pacing and lattice constant values for NbP supported catalysts were observed in comparison with the parent SBA-15, parameter values decreased about 0.55-0.73nm and 0.64-0.68 nm, respectively (Table 1). The pore wall thickness for the catalysts NbP-A/SBA-15, NbP-B/SBA-15 and NbP-D/SBA-15 increased about 0.89 and 0.39 and 1.08nm, respectively, clearly evidencing the dispersion of NbP nanoparticles inside the mesoporous channels. However, the catalyst NbP-C/SBA-5 prepared at 80 °C under concentrated HCl solutions showed significant impact on pore wall thickness of the material and decreased about 0.77nm. This observation was in agreement with the B.E.T. results (see below), since the pore sizes increased about 0.09 nm in contrast to the parent SBA-15 support. Nevertheless, this effect was not observed in the case of the NbP-D/SBA-15 catalyst prepared under concentrated HCl solutions at room temperature. Wide angel X-ray diffraction pattern shown in Fig. 1b revealed that the NbP particles dispersed on NbP-A and NbP-B/SBA-15 did not show any diffractions and thus might correspond to NbP particles being amorphous in nature. In the case of NbP-C/SBA-15, NbP-D/SBA-15 and NbP-bulk catalysts (Fig 1b and Fig. 5Sc), several well-defined reflections appeared around 2θ of 19.8° (110), 25.6° (101), 27.9° (200) 39.9° (220), 44.7° (310) and 47.9° (301), respectively, which were ascribed to niobium oxyphosphate ($NbOPO_4$) crystalline phases and the pattern was in a good agreement with the reported literature[22,34]. The intensity of these peaks were increased with increasing amounts of NbP (5, 10 and 20%) loading over the support (ESI, Fig.S5b) and revealing that the SBA-15 support reasonably retaining its structure upon loading of 20%NbP (ESI, S1a). Consequently, no phase changes were observed on the NbP-C/SA-15 catalyst upon

calcination at different temperatures ranging from 300, 400 and 500 °C, thus indicating the thermal stability of the catalysts (ESI, Fig. S5d).

3.1.2. N_2-adsorption-desorption

N_2-adsorption-desorption measurement were carried out for the support and the supported NbP catalysts, the corresponding isotherms and the pore size distribution curves are shown in Figs.2a and 2b, respectively. The surface area, pore size and pore volume for the studied catalysts are presented in Table 1. The representative type IV isotherm observed for the mesoporous SBA-15[32] support (Fig.2a) was not significantly affected upon loading niobium oxyphosphate even when using different preparation conditions. However, the NbP-C/SBA-15 catalyst prepared using concentrated HCl conditions gave rise to a slight change in the hysteresis loop (type H1) and shifted towards a higher partial pressure. The changes in the hysteresis loop might be the result of surface etching by HCl, thereby increasing the pore size (Fig 2b and Table 1). The decrease in the pore size and increase in the pore wall thickness were observed in the case of NbP-A/SBA-15, NbP-B/SBA-15 and NbP-D/SBA-15 catalysts thus evidencing the coating of NbP nanoparticles inside the mesoporous channels. Interestingly, the surface area and pore volume obtained the spent catalyst remained same as compared with fresh catalyst after several reuses enlightening the stability of the catalysts under the studied reaction conditions (Table 1).

3.1.3. FT-IR and ^{31}P-MAS-NMR

Infrared spectra (FT-IR) for the catalysts prepared under different conditions and the NbP-C/SBA-15 catalyst with different amounts of NbP loading (5, 10 and 20 wt.%) are shown in Figs. 3a and Fig. 3b, respectively. The catalysts exhibited a broad band centered around 3500 cm^{-1} and 1630 cm^{-1}, respectively, and are characteristic stretching vibrations evidence the presence of different hydroxyl groups such as physisorbed water molecules, bridged hydroxyl (Si-O(H)-Si and surface silanol groups, respectively[35]. A sharp peak observed around at 3741

cm^{-1} and the shoulder around 3663 cm^{-1} are assigned to the stretching vibrations for the isolated hydroxyl (Si-OH and Nb-OH) and P-OH groups, respectively[35,36]. The bands appearing around 1070-1200, 800 and 460 cm^{-1} are due to asymmetric, symmetric and bending vibrations of the Si-O-Si bridged atoms and are characteristic bands for Si-SBA-15 materials[35]. The new signals appeared around the region 540-640, 920 and 1000-1200 cm^{-1} comparing with Si-SBA-15 support confirms the presence of NbP species on the support. Sharp bands appeared around 585 and 633cm^{-1}, respectively, in comparison with Si-SBA-15 can be assigned to Si-O-Nb and Nb-O-P or P-OH stretching vibrations respectively. These observations are consistent with the presence of NbP species bonded with the silica (SBA-15) support[30,37,38]. The bulk NbP catalyst gave rise to a strong band at 1033cm^{-1} due to the stretching vibrations for phosphate species (O═P═O or Nb-O-P), however, this peak is overlapped with Si-O-Si bands in the case of supported NbP catalysts. Further, the intensity of 1033cm^{-1} peak increased with an increase in the NbP loading confirming the presence of phosphate species in the form of niobium oxyphosphate over the support (Fig. 3b). The increase in intensity of the broad band appeared around 3500cm^{-1} for the adsorbed water molecule was observed in the case of NbP loaded catalysts which also confirms the coverage of hydrophilic NbP species over the mesoporous channels. Small bands observed around 2858 and 2961cm^{-1}, respectively, for the spent catalyst due to the asymmetric and symmetric vibrations of C-H bonds for the chemisorbed organic molecules over the active sites of the catalysts.

The local environment and the connectivity of the phosphate species attached to niobium over SBA-15 surface was studied by means of ^{31}P-MAS-NMR and the results are depicted in Fig. 4. The NbP-bulk and NbP-B and NbP-C/SBA-15 catalysts give rise to strong resonance peaks around 19.0-23.0 ppm with respect to 85% aq H_3PO_4 (characteristic chemical shift for $NbOPO_4$) that are likely attributed to the Q_2 and Q_3 type tetrahedral coordinated phosphorus sites neighbouring the niobium sites and thus confirming the presence of phosphorous as in the form

of $NbOPO_4$ over the SBA-15 surface[39]. On the contrary, the NbP-A/SBA-15 catalyst prepared with no HCl gave rise to a broad peak around -9 ppm, in contrast to other catalysts prepared under HCl conditions due to phosphorous present in the Q1 type coordination which has been assigned to the terminal type phosphates.

3.1.4. XPS results

The XPS spectra obtained for bulk NbP, fresh and spent NbP-C/SBA-15 catalysts, the deconvoluted Nb3d and P2p curves are presented in Figs. 5 and 6, respectively. The bulk NbP catalysts give rise to peaks centered around 133.0 and 207.1 eV, respectively, attributed to the binding energy values for $P2p_{3/2}$ and $Nb3d_{5/2}$. All these peaks were also observed for the fresh and spent NbP-C/SBA-15 suggesting the presence of P and Nb in the form of $NbOPO_4$ on the surface of Si-SBA-15 support. The binding energy values of 133.0 ($P2p_{3/2}$) and 207.1 eV ($Nb3d_{5/2}$) obtained for bulk $NbOPO_4$ catalyst were slightly shifted towards higher binding energy side in the case of the NbP supported on SBA-15 catalysts (133.2 and 207.4 eV for fresh and 133.3 and 207.6 eV for spent catalyst) thus explaining the interaction of Nb with the support there by the formation the Si-O-Nb linkages ($Si\text{-}O\text{-}NbOPO_4$)[36].

3.1.5. NH_3-TPD results

The total acidity of NbP/SBA-15 catalysts prepared under different synthesis conditions and different amounts of NbP loaded on the catalyst supports were studied by the NH_3-TPD method and the results are shown in Fig. 7. It was observed that both bulk NbP and 10wt%NbPx/SBA-15 (where, x = method A, B, C and D) catalysts prepared under different conditions. demonstrated a broad peak around the temperature range of 100-450 °C, indicating the presence of both weak and medium strength acid sites. However, the total acidity and the amount of weak and medium acid sites varied upon preparation conditions. The catalysts prepared at 80 °C with no HCl (NbP-A) and with 1.0M HCl (NbP-B) exhibited a strong peak around 200 °C similar to

the Nb_2O_5/SBA-15 sample, this indicating the presence of more weak acid sites attributed to Nb_2O_5 species. On the other hand, the supported catalyst prepared at room temperature, (NbP-D/SBA-15) and 80 °C (NbP-C/SBA-15) with concentrated HCl gave rise to a strong peak around 350 °C due to the presence of more medium strength acid sites. The weak and medium acid sites are likely due to the presence of different species. The presence of weak acid sites in the former case might be resulting from the presence of Nb_2O_5 species formed upon aggressive hydrolysis of niobium precursor resulting in the formation of bigger aggregates, niobium being present inside the aggregates which may not be converted into Nb-O-PO_4. The unconverted $Nb(OH)_5$ species inside the cluster could be converted into Nb_2O_5 upon calcination comprising low-coordinated Nb sites (Nb^{5+}, Lewis sites). The Nb_2O_5 being in strong interaction with the acidic surface of the support (Si-$OH2^+$), results in the formation of highly distorted NbO_6 octahedral that possesses short Nb=O bonds and is responsible for the Lewis acid sites (weak acid sites).[40-42] The new peak observed around 922 cm^{-1} in the FT-IR spectra also confirms the presence of this short Nb=O species over the surface. This observation is further evidenced by the SEM images shown in Fig. 9. The increased amount of medium acid sites in the latter case might be the deposition of Nb in the form of NbOPO4 over SBA-15 surface and resulting in an increased number of Si-O-Nb-O-PO_4 and Nb-OH sites which are associated with Brønsted acid sites.[36,43] The amount of acid sites over the studied catalysts follows the order Nb_2O_5/SBA-15> NbP-B/SBA-15 > NbP-A/SBA-15 > NbP-D/SBA-15 > NbP-C/SBA-15. The TPD profile for 5, 10 and 20%NbP loaded SBA-15 catalysts (not shown) and the total acidity follows the order 20%NbP > 10%NbP > 5%NbP/SBA-15 catalysts. The number of acid sites increased with increasing NbP loading up to 10wt.%NbP and this might result from better dispersion of niobium without significantly affecting the surface properties of the support. The amount of acid sites decreased in the case of 20%NbP loaded catalyst due to a drastic decrease in the

surface area and pore volume of the support and the formation of larger aggregates that restricts the amount of exposed acid sites over the surface.

3.1.6. TGA results

The thermal stability of the calcined Si-SBA-15, NbP-C/SBA-15 and spent NbP-C/SBA-15 catalysts were studied by Thermogravimetric Analysis (TGA) and the results are presented in Fig. 8. The support and NbP-C/SBA-15 catalyst show weight losses in two temperature regions: 50-120 °C and 120-735 °C, respectively. The initial weight loss of about 2% for the support and 5.6% for NbP-C/SBA-15 catalyst observed in the first temperature region was due to desorption of physisorbed water molecules. No distinct endotherm was observed in the second temperature region but, however, the weight loss of about 6 and 5.4% was observed for the support and NbP-C/SBA-15 catalyst, respectively, due to the removal of water molecules by siloxane bond formation via silanol condensations. About 3.6% higher weight loss was observed in the first temperature region while subtracting the weight loss of the NbP-C/SBA-15 from Si-SBA-15 support might be the coverage of hydrophilic NbP species that absorbs more water molecules over the surface. About 0.8% lower weight loss was observed in the second temperature region and the reason could be a decrease in the amount of silanol groups over the surface due to the formation of Si-O-Nb bonds of NbP and Nb_2O_5 species. This observation is also in a good agreement with the FT-IR results. In the case of spent catalyst, the first isotherm looks similar as that of the fresh catalysts (5.6% weight loss) but the second isotherm gives rise to a total weight loss of about 17.4% around the temperature region 400-500 °C (12.4% more in comparison with fresh catalyst) due the removal of accumulated reaction products over the active sites. The FT-IR results also evidenced the presence of organic molecules on the spent catalyst (Fig.3a). TGA results revealed that the supported NbP-C/SBA-15 was very stable at very high temperatures and under studied reaction conditions. Further, the

FT-IR and X-ray diffraction patterns for the NbP-C/SBA-15 catalysts also show no phase changes upon calcination at different temperatures ranging from 300-500 °C (Fig. S5d).

3.1.7. SEM-EDX and TEM

The surface morphology and the dispersion of Nb and P for the studied catalysts were examined by means of SEM-EDX and the images are shown in Figs. 9 and 10. It was evident that the worm/rod like surface morphology of Si-SBA-15 (Fig. 9) was not much affected by the synthesis conditions used for NbP deposition in contrast with the other reported literature where use of concentrated H_3PO_4 destroyed up to 90% of the surface area and pore volume of the support.[44] In our preliminary studies, similar results were also obtained for the catalyst $NbOPO_4$/SBA-15 obtained by H_3PO_4 treatment method, the surface area of the support Si-SBA-15 decreased abruptly to 367 m^2/g and severely altered the pore architecture of the support. (ESI, Fig. S6a). The NbP-A/SBA-15 and NbP-B/SBA-15 catalysts display the dispersion of NbP particles with some bigger aggregates over the surface and it appears that the particles were amorphous in nature. Further examination by EDX microelement mapping also explains the formation of larger aggregates since these catalysts show the Nb/P ratio of 1.12 and 2.36, respectively, revealing that the catalysts contain more niobium than phosphates and the aggregates might be mainly composed of Nb_2O_5 species (ESI Fig. S7). In the case of NbP-C/SBA-15 catalysts, the surface was smooth and almost identical to the parent SBA-15 carrier, although, the close view of EDX microelement mapping of this sample show very uniform dispersion of Nb and P over the surface with Nb/P ratio of 1.02 explaining the presence of niobium and phosphate together on the surface (Fig. 10c and Fig. S7) . However, in some places flower like particles were observed over the external surface and appeared to be crystalline in nature (ESI, Fig. S6b). This could be the reason for obtaining well defined diffraction pattern characteristics of niobium oxyphosphate in XRD (Fig. 1b). In the case of NbP-D/SBA-15

catalysts, SEM images depict different morphology and uniform film-like NbP particles were observed over the surface; the particles appeared to be semi-crystalline and EDX mapping demonstrated very uniform distribution of Nb and P, in this case with Nb/P ratio of about 1.04. The pore architecture of the support Si-SBA-15, NbP/SBA-15 and palladium containing NbP/SBA-15 catalysts was examined by means of TEM and the images are shown in Fig.11. It can be clearly seen that the Si-SBA-15 was formed with well aligned and regular arrangements of hexagonal mesopores and the regularity of these mesopores are not affected and was very well preserved after loading 10wt.% of NbP and 5wt.% of palladium over the surface. Fig. 11b and 11c&d exemplify the coverage of niobium oxyphosphate over Si-SBA-15 surface and the homogeneous dispersion of Pd nanoparticles over NbP/SBA-15 catalysts achieved by means of simple incipient wetness method.

3.2. Catalytic activity

3.2.1. Hydroxyalkylation/alkylation reaction (HAA) results

3.2.1.1. Effect of catalyst

The catalytic activity of all the NbP supported SBA-15 catalysts prepared at different conditions were initially investigated upon solventless hydroxyalkylation/alkylation of 1-butanal with 2-methyl furan to produce jet-fuel range hydrocarbon precursors. The performance of these catalysts was further compared with home-made Al-SBA-15 and Nb_2O_5/SBA-15 (niobic acid) and commercial ZSM-5 catalysts and the results are presented in Table 2 and Fig. 12a. All four NbP/SBA-15 catalysts prepared under different conditions gave rise to superior activity in the hydroxyalkylation/alkylation reaction of 1-butanal with 2-MF in comparison to Nb_2O_5/SBA-15, Al-MCM-41 and commercial ZSM-5 catalysts. The observed trend of TOF was consistent with the combined effects of acid site strength and its concentration (Fig 12b). The catalysts NbP-A and NbP-B/SBA-15, presenting weaker acid sites (prepared without and with 1M HCl)

slightly underperformed in terms of aldehyde conversion (85.5 and 87.2% respectively) compared with the NbP-C and NbP-D/SBA-15 catalysts (99.6 and 98.8% respectively) prepared with concentrated HCl conditions presenting stronger acid sites. Most importantly, the

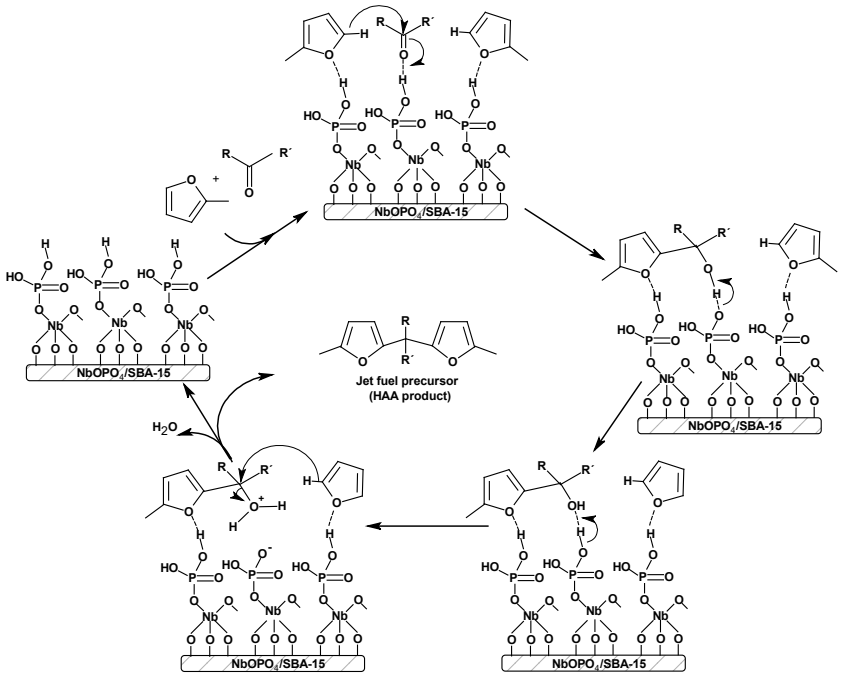

Scheme 2. Proposed reaction mechanism for the formation of jet-fuel precursor over NbP/SBA-15 catalyst via hydroxyalkylation/alkylation of bio-based carbonyls with 2-methyl furan.

TOF and the catalytic activity of the SBA-15 supported NbP catalysts were almost two times higher when comparing with bulk NbP catalyst prepared under similar conditions. Nb_2O_5/SBA-15 and Al-MCM-41 catalysts were underperformed owing to the lack of strong acid sites, on the other hand, highly acidic ZSM-5 displayed poor aldehyde conversion (16.4% in 5h) among the studied catalysts due to mass transfer limitations (narrow pores) restricts its use in reactions involving larger molecules and enlightens the importance of mesoporous NbP/SBA-15

catalysts (outperformed in HAA of carbonyls with 2-MF). Furthermore, based on the experimental findings, one can conclude that the hydroxyalkylation/alkylation requires strong Brønsted acid sites to catalyse the reaction via the carbocation mechanism depicted in Scheme 2, this observation is in agreement with the findings in literature.[45]

3.2.1.2. ~~Effect~~ Influence of reaction parameters

The most active NbP-C/SBA-15 (in terms of 1-butnal conversion) was further chosen to optimize reaction parameters such as temperature, reaction duration, reactants/catalyst mass ratio, NbP loading and catalyst calcination temperature to achieve maximum carbonyl conversion and selectivity towards the HAA oxygenates (ESI, Fig. S8). The effect of reaction temperature (40-60 ºC) is presented in supporting Figs. S8a and S8b, shows that complete conversion with HAA selectivity ≥93% could be reached in 3-5 h at temperatures 50-60 ºC. In terms of NbP loading, 10% loading was found to be optimum (highest TOF) and also as 10 and 20% NbP loaded catalysts perform similarly in terms of HAA product selectivity in 5 h (Figs. S8c and S8d). The aldehyde conversion did not increase with an increase in the NbP loading above 10% and this observation clearly explained the role of NbP dispersion over the surface. This is also in agreement with the surface properties obtained by BET, TPD and SEM-EDX techniques, respectively. The surface acidity increased with increasing NbP loading up to 10 wt.% (69 and 131 µmol/g for 5 and 10wt.%NbP, respectively). However, only a small increase in acidity was obtained for the 20% NbP catalyst (163 µmol/g) due to drastic decline in the surface properties of the support such as surface area and pore volume (loss of 56.6% of the surface area and 53.8% of the pore volume) leading to the formation of bigger aggregates of NbP over the surface serves less amount of surface exposed acid sites. The results revealed that these catalysts gave rise to a better stability, NbP dispersion and catalytic activity upto 10wt.% of NbP loading. The catalyst calcination temperature (calcined at different temperatures ranging

from 300 to 500 ºC) was not too prominent and similar aldehyde conversions and HAA product selectivities were reached (Figs. S8e and S8f). The results obtained from catalytic experiments in a polar reaction medium and the characterization results obtained by XRD, TGA and B.E.T., respectively, proved the superior thermal and hydrothermal stability of the NbP/SBA-15 catalysts. The effect of catalyst mass vs reactants amount over the conversion of butanal was studied at 50 ºC keeping the catalyst mass constant (50 mg), varying the amount of reactants (2.5, 3.75 and 5mmol respectively) and the results are presented in Figs. S8g and S8h. The results revealed that the aldehyde conversion was decreased about 10% in the beginning of the reaction (1h of reaction time) by doubling the reactants amount (2.5mmol to 5 mmol) and reached almost full conversion in 5h of reaction time demonstrating the superior activity of NbP/SBA-15 catalysts.

3.2.1.3. ~~Effect~~ Influence of carbonyl compound

The performance of NbP-C/SBA-15 catalyst was further proven upon the reaction of other biomass derived aldehydes and ketones (furfural, acetone and cyclohexanone) with 2-MF under optimized reaction conditions and the results are presented in Table 3 and Figs. S9a and S9b (ESI). The results clearly depict the difference in reactivities of the carbonyl compounds used. The observed reactivity trend was in agreement with the trends found in literature and consistent with the steric and electronic effects of carbonyl compounds that determine the formation/ stability of carbocation intermediates[45]. The reactivity trend in decreasing order of TOF as well as carbonyl conversion was as follows: butanal > furfural > cyclohexanone > acetone. Butanal conversion of about 97.5 % with HAA selectivity of about 93% was reached in 3h at 60 ºC, the results thus obtained herein for NbP-C/SBA-15 show significant improvement over mesoporous $NbOPO_4$ catalysts reported by Xia *et al.*, presenting 95.3% butanal conversion and 89.5% HAA yield in 5h at 80 ºC. The superior activity of supported NbP-C/SBA-15 catalyst

likely arises from the uniform distribution of NbP particles and of well-exposed acid sites over the high surface area mesoporous carrier. Also, in case of furfural, cyclohexanone and acetone, better conversion at lower temperature (60 ºC) could be obtained than in the study of Xia *et al.* Carbonyl conversion of about 79.8, 51.4 and 32,6% and HAA selectivity of about 81.4, 91 and 81.1%, respectively, was obtained in 5h of reaction time (a carbonyl conversion of about 86.8, 96.6 and 79.1% and HAA selectivity of about 81.7, 91.5 and 82.1%, respectively, was achieved in 24h of reaction time).

3.2.1.4. Catalyst reusability

In order to study the operational stability of supported NbP/SBA-15 catalysts, reusability of NbP-C/SBA-15 catalyst was investigated upon hydroxyalkylation/alkylation of butanal with 2-MF at optimized reaction conditions (60 ºC, 3h reaction time). To conduct reusability tests the catalyst was separated by centrifugation after every run, washed several time with methanol, dried at 100 ºC and reused in the next run. The results of reuse experiments depicted in Fig.13 shows that the carbonyl conversion decreased from 97.5% (first run) to 87.1, 86.4 and 82.9% in the second and third recycle, respectively, revealed that the activity of the catalyst lost about 10.3% in the first recycle and only 0.7 and 3.5% in second and thirst recycle show the stability of the catalyst. The activity loss during first recycle might not be leaching of acid sites since according to the TPD results similar amount of total acid sites could be found as in the case of fresh catalyst. On the basis of FT-IR results, it seems that strongly chemisorbed reaction products remain on the active sites and render the active sites unavailable for the reaction. A higher level of weight loss in comparison with fresh catalyst around the temperature region of 300-500 ºC was also observed by TGA which could be attributed to the removal of chemisorbed reaction products. Also, the peaks observed by FT-IR around 2900 cm^{-1} for the C-C bond stretching vibrations confirms the presence of chemisorbed organic molecules. Overall, the

catalyst was very stable under the studied reaction conditions and the catalytic activity could be restored to 100% via intensive washing or by recalcining the spent catalyst to remove adsorbed organic molecules.

3.2.2. Hydrodeoxygenation (HDO) results

The unique acid properties of NbP/SBA-15 catalysts prepared under different experimental conditions were further explored for the fabrication of bifunctional Pd-NbP/SBA-15 catalysts by introducing 5wt.% Pd through incipient wetness impregnation method. All the Pd containing NbP/SBA-15 catalysts were further utilized upon the hydrodeoxygenation (HDO) of HAA products at 50 bar hydrogen pressure and 200 ºC, using cyclohexane as a solvent. The results of HDO experiments summarized in Table 4 clearly demonstrate the superior activity of bifunctional Pd-NbP/SBA-15 over the monofunctional commercial Pd/C catalyst. Among, the different bifunctional Pd catalysts (Pd/NbP-A, Pd/NbP-B, Pd/NbP-C/SBA-15, Pd/bulk NbP and Pd/Nb_2O_5/SBA-15) the Pd containing NbP catalysts Pd/NbP-B, Pd/NbP-C/SBA-15 and Pd/bulk NbP presented comparable deoxygenation activity (100% hydrodeoxygenation). These bifunctional catalysts produced C9-C14 jet-fuel range branched hydrocarbon products via hydrogenation, ring opening, catalytic cracking and isomerization pathways. Most importantly, with these catalysts, total hydrocarbon selectivity of about 100% and branched C14 hydrocarbon selectivity of about 56.4 and 48.4 and 26.3% could be reached in 12 h respectively (entries 2, 3 and 6). Under identical experimental conditions, Pd/NbP-A/SBA-15 and Pd/Nb_2O_5/SBA-15 catalysts gave only 77.9 and 44.7% total hydrocarbon selectivity and double bond saturated products selectivity of about 55.3 and 20.1%, respectively. Commercial Pd/carbon catalyst gave rise to no hydrodeoxygenation activity at 200 ºC due to lack of acidic sites for ring opening and formed only the hydrogenated furanics. However, an increase in the reaction temperature to 250 ºC in the case of Pd/NbP-A/SBA-15 and 300 ºC in the case of

Pd/carbon catalysts produced 100 % deoxygenated products with C14 hydrocarbon selectivity of about 53.1 and 52.3%, respectively. On the basis of these observations, one can conclude that the Pd/NbP-B and Pd/NbP-C/SBA-15 catalysts containing strong acid sites (more Brønsted acid sites) were more active upon the deoxygenation of long chain furanics and the reaction proceeded under much mild conditions (200 ºC) than monofunctional catalysts. On the other hand, Pd/NbP-A, Nb_2O_5/SBA-15 catalysts containing weaker Lewis acid sites and Pd/carbon catalyst with no acid sites required high temperatures (>250 ºC) to promote thermal ring opening and remove oxygen from HAA products. Therefore, it can be concluded that the deoxygenation reaction proceeds via a bifunctional reaction mechanism (hydrogenation over metal sites and ring opening, cracking and isomerisation over acid sites). The catalysts Pd/NbP-B and Pd/NbP-C/SBA-15 contained optimal bifunctional properties and gave jet-fuel range hydrocarbons with 100% selectivity. Further, the amount and strength of acid sites plays an important role in the C14 hydrocarbon selectivity. The catalyst Pd/NbP-B/SBA-15 show less cracking and gave the maximum C14 hydrocarbon selectivity of about 56.3%. In comparison to other bifunctional catalysts, the performance towards C14 hydrocarbons follows the order; Pd/NbP-B/SBA-15 > Pd/NbP-A/SBA-15 > Pd/NbP-C/SBA-15 > Pd/Nb_2O_5/SBA-15 > Pd/bulk NbP. On the other hand, 10%NbP containing SBA-15 catalysts performed better in terms of C14 hydrocarbon selectivity compared to 5 and 20% NbP containing SBA-15 catalysts (Table 4, entries 3, 4 and 5). Thus, it can be concluded that the catalysts containing an optimal amount of both weak and medium acid sites performed well in terms of obtaining the desired branched C14 hydrocarbons (jet-fuel range). Also, the influence of reaction time on the hydrodeoxygenation of C14-HAA was studied in order to achieve maximum C14 hydrocarbon selectivity and the results are given in Table 4 (entry 2). The obtained results clearly show that the reaction proceeded via double bond saturation, deoxygenation and catalytic cracking; The C14 selectivity increased with longer reaction time up to 8h and decreased upon further increase

in the reaction time (23.3, 67 and 56.4 % C14 hydrocarbon selectivities in 4, 8 and 12 hours, respectively). Hydrodeoxygenation of the other HAA products were also investigated with the optimum deoxygenation catalyst under identical experimental conditions which showed similar trends of activities and total hydrocarbon selectivities of about 100% in the case of cyclohexanone HAA/acetone HAA oxygenates and 89.1% in the case of furfural HAA oxygenate. (Table 3, entries 9, 10 and 11).

4. CONCLUSIONS

An effective and liquid H_3PO_4 free hydrothermal method is presented for obtaining highly dispersed, high surface area and active mesoporous $NbOPO_4$/SBA-15 catalysts. The activity of Brønsted acidic NbP ($NbOPO_4$) sites were significantly enhanced resulting from the improved dispersion of NbP species over high surface area mesoporous SBA-15 structure. Most importantly, the acidic properties of NbP/SBA-15 catalysts are easily tuneable (weak to medium acid sites) and the characterization results revealed that the structural features of SBA-15 remained intact in the supported catalysts. The performance of the prepared catalysts was demonstrated upon the synthesis of renewable jet-fuel range hydrocarbons precursors via HAA of various bio derived furanics and subsequent hydrodeoxygenation of the HAA products into fuel range hydrocarbons over metal loaded bifunctional 5% Pd-NbP/SBA-15 catalysts. The NbP-C/SBA-15 catalyst prepared in concentrated HCl conditions possessed more medium acid sites that were well dispersed over the support, these catalysts were highly active upon hydroxyalkylation/alkylation reaction and overcomes the drawbacks of Al-SBA-15 and ZSM-5 catalysts. Also, the catalytic activity was two times higher in terms of TOF when comparing with the bulk NbP catalyst prepared under identical conditions. Further, the 5% Pd loaded NbP/SBA-15 catalysts showed superior activity and selectivity upon subsequent hydrodeoxygenation of HAA products into jet-fuel range hydrocarbons outperforming the

commercial Pd/carbon, Pd/NbPbulk and Pd/Nb_2O_5/SBA-15 catalysts. It can be concluded that the superior catalytic activity and advanced surface properties of the NbP/SBA-15 ($NbOPO_4$) catalysts presented here could also find other potential applications in industrial use exclusively in the valorisation of bio-based large organic molecules into value added products and alternative to the conventional homogeneous catalysts.

AKNOWLEGMENTS

The Bio4Energy programme, Kempe Foundations (Kempe stiftelserna) and Wallenberg Wood Science Center (WWSC) are gratefully acknowledged. The authors acknowledge the facilities of Umeå Core Facility Electron Microscopy (UCEM) and the technical assistance of Dr. Tobias Sparrman, Chemical Biological Centre (KBC), Umeå University. This work is also a part of the Johan Gadolin Process Chemistry Centre at Åbo Akademi University.

Formatted: English (United States)

Field Code Changed

REFERENCE

[1] Corma, A.; Iborra, S.; Velty, A., Chemical Routes for the Transformation of Biomass into Chemicals. *Chem. Rev.* **2007**, 107, 2411–2502.

[2] Demirbas, M. F.; Balat, M., Recent Advances on the Production and Utilization Trends of Bio-fuels: A Global Perspective. *Energy Convers. Manage.* **2006**, 47, 2371–2381.

[3] Mohr, A.; Raman, S., Lessons From First Generation Biofuels and Implications for the Sustainability Appraisal of Second Generation Biofuels. *Energy Policy*. **2013,** 63, 114–122.

[4] Al-Zuhair, S., Production of Biodiesel: Possibilities and Challenges. *Biofuels Bioprod. Biorefin.* **2007**, 1, 57–66.

[5] Luque, R.; Herrero-Davila, L.; Campelo, J. M.; Clark, J. H.; Hidalgo, J. M.; Luna, D.; Marinas, J. M.; Romero, A. A., Biofuels: a Technological Perspective. *Energy Environ. Sci.* **2008**, 1, 542–564.

[6] Chheda, J. N.; Huber, G. W.; Dumesic, J. A., Liquid-phase Catalytic Processing of Biomass-derived Oxygenated Hydrocarbons to Fuels and Chemicals. *Angew. Chem. Int. Ed.* **2007,** 46, 7164–7183.

Field Code Changed

Field Code Changed

Field Code Changed

[7] Li, G.; Li, N.; Wang, X.; Sheng, X.; Li, S.; Wang, A.; Cong, Y.; Wang, X.; Zhang, T., Synthesis of Diesel or Jet Fuel Range Cycloalkanes with 2-Methylfuran and Cyclopentanone from Lignocellulose. *Energy Fuels*. **2014,** 28, 5112–5118.

[8] Li, G.; Li, N.; Li, S.; Wang, A.; Cong, Y.; Wang, X.; Zhang, T., Synthesis of Renewable Diesel with Hydroxyacetone and 2-Methyl-furan. *Chem. Commun.* **2013**, 49, 5727–5729.

[9] Hronec, M.; Fulajtárova, K.; Liptaj, T.; Štolcová, M.; Prónayová, N.; Soták, T.; Cyclopentanone: A Raw Material for Production of C15 and C17 Fuel Precursors. *Biomass Bioenergy.* **2014,** 63, 291–299.

[10] Corma, A.; Torre O.; Renz, M., Production of High-Quality Diesel from Cellulose and Hemicellulose by the Sylvan Process: Catalysts and Process Variables. *Energy Environ. Sci.* **2012,** 5, 6328–6344.

[11] Li, H.; Saravanamurugan, S.; Yang, S.; Riisager, A., Catalytic Alkylation of 2-Methylfuran with Formalin Using Supported Acidic Ionic Liquids. *ACS Sustain. Chem. Eng.* **2015,** 3, 3274−3280.

[12] Li, G.; Li, N.; Li, S.; Wang, A.; Cong, Y.; Wang, X.; Zhang, T., Synthesis of Renewable Diesel Range Alkanes by Hydrodeoxygenation of Furans Over Ni/Hβ Under Mild Conditions, *Green Chem.* **2014**, 16, 594−599.

[13] Li, G.; Li, N.; Li, S.; Wang, A.; Cong, Y.; Wang, X.; Zhang, T., Synthesis of Renewable Diesel with Hydroxyacetone and 2-Methyl-Furan. *Chem. Commun.* **2013,** 49, 5727−5729.

[14] Climent, M. J.; Corma, A.; Iborra, S., Conversion of Biomass Platform Molecules into Fuel Additives and Liquid Hydrocarbon Fuels. *Green Chem.,* **2014,** 16, 516−547.

[15] Deng, Q.; Han P.; Xu, J.; Zou, J. J.; Wang, L.; Zhang, X., Highly Controllable and Selective Hydroxyalkylation/Alkylation of 2-Methylfuran with Cyclohexanone for Synthesis of High-Density Biofuel. *Chem. Eng. Sci.* **2015,** 138, 239–243.

[16] Sutton, A. D.; Waldie, F. D.; Wu, R.; Marcel, S.; Pete, S. L. A.; Gordon, J. C., The Hydrodeoxygenation of Bioderived Furans into Alkanes, *Nat. Chem.* **2013,** 5, 428–32.

[17] Wang, T.; Li, K.; Liu, Q.; Zhang, Q.; Qiu, S.; Long, J.; Chen, L.; Ma, L.; Zhang, Q., Aviation Fuel Synthesis by Catalytic Conversion of Biomass Hydrolysate in Aqueous Phase. *Appl. Energy,* **2014,** 136, 775–780.

[18] Li, S.; Li, N.; Li, G.; Li, L.; Wang, A.; Cong, Y.; Wang, X.; Zhang, T., Lignosulfonate-Based Acidic Resin for the Synthesis of Renewable Diesel and Jet Fuel Range Alkanes with 2-Methylfuran and Furfural. *Green Chem.* **2015,** 17, 3644–3652.

[19] Xia, Q-N.; Cuan, Q.; Liu, X-H.; Gong, X-Q.; Lu, G-Z.; Wang, Y-Q., Pd/$NbOPO_4$ Multifunctional Catalyst for the Direct Production of Liquid Alkanes from Aldol Adducts of Furans. *Angew. Chem. Int. Ed.* **2014,** 53, 9755–9760.

[20] Nowak, I.; Ziolek, M.; Niobium Compounds: Preparation, Characterization, and Application in Heterogeneous Catalysis. *Chem. Rev.* **1999,** 99, 3603–3624.

[21] Nakajima, K.; Baba, Y.; Noma, R.; Kitano, M.; Kondo, J. N.; Hayashi, S.; Hara, M., $Nb_2O_5.nH_2O$ as a Heterogeneous Catalyst with Water-Tolerant Lewis Acid Sites. *J. Am. Chem. Soc.* **2011,** 133, 4224–4227.

[22] Weng, W.; Davies, M.; Whiting, G.; Solsona, B.; Kiely, C.; Carley, A. F.; Taylor, S. H., Niobium Phosphates as New Highly Selective Catalysts for the Oxidative Dehydrogenation of Ethane. *Phys. Chem. Chem. Phys.* **2011,** 13, 17395–17404.

[23] Gao, J. L.; Gao, S.; **Liu**, C. L.; Liu, Z. T.; Dong, W. S., Synthesis, Characterization, and Catalytic Application of Ordered Mesoporous Carbon–Niobium Oxide Composites., *Mat. Res. Bull.* **2014,** 59, 131–136.

[24] García-Sancho, C.; Agirrezabal-Telleria, I.; Güemez, M. B.; Maireles-Torres, P., Dehydration of d-Xylose to Furfural Using Different Supported Niobia Catalysts. *Appl. Catal. B: Environ.* **2014,** 152-153, 1–10.

[25] Bozzi, A. S.; Lavall, R. L.; Souza, T. E.; Pereira, M. C.; De Souza, P. P.; De Abreu, H. A.; De Oliveira, A.; Ortega, P. F. R.; Paniago, R.; Oliveira, L. C. A., An Effective Approach for Modifying Carbonaceous Materials with Niobium Single Sites to Improve Their Catalytic Properties. *Dalton Trans.* **2015,** 44, 19956-19965.

[26] Prasetyoko, D.; Ramli, Z.; Endud, S.; Nur, H., Characterization and Catalytic Performance of Niobic Acid Dispersed over Titanium Silicalite. *Adv. Mater. Sci. Eng.* **2008,** Article ID 345895, 1-12.

[27] Zhang, Y.; Wang, J.; Ren, J.; Liu, X.; Li, X.; Xia, Y.; Lu, G.; Wang, Y., Mesoporous Niobium Phosphate: an Excellent Solid Acid for the Dehydration of Fructose to 5-Hydroxymethylfurfural in Water. *Catal. Sci. Technol*. **2012,** 2, 2485–2491.

[28] Mal, N. K.; Bhaumik, A.; Kumar, P.; Fujiwara, M., Microporous Niobium Phosphates and Catalytic Properties Prepared by a Supramolecular Templating Mechanism, *Chem. Commun.* **2003,** 872–873.

[29] Mal, N. K.; Fujiwara, M., Synthesis of Hexagonal and Cubic Super-Microporous Niobium Phosphates with Anion Exchange Capacity and Catalytic Properties. *Chem. Commun.,* **2002,** 2702–2703.

[30] Francisco, M. S. P.; Cardoso, W. S.; Gushikem, Y.; Landers, R.; Kholin, Y. V., Surface Modification with Phosphoric Acid of SiO_2/Nb_2O_5 Prepared by the Sol-Gel Method: Structural-Textural and Acid Sites Studies and an Ion Exchange Model. *Langmuir* **2004,** 20, 8707–8714.

[31] Li-wei, Z.; Jian-Gang, W.; Ping-Ping, Z.; Feng, S.; Xiu-Yu. S.; Li-Hong, W.; Hong-You C.; Wei-Ming, Y., Preparation of the Nb-P/SBA-15 Catalyst and its Performance in the Dehydration of Fructose to 5-Hydroxymethylfurfural. *J. Fuel Chem. Technol.* **2017,** 45, 651–659.

[32] Zhao, D.; Huo, Q.; Feng, J.; Chmelka, B. F.; Stucky, G. D., Nonionic Triblock and Star Diblock Copolymer and Oligomeric Surfactant Syntheses of Highly Ordered, Hydrothermally Stable, Mesoporous Silica Structures. *J. Am. Chem. Soc.* **1998**, 120, 6024–6036.

[33] Samikannu, A.; Golets, M.; Larsson, W.; Shchukarev, A.; Kordas, K.; Leino, A.-R.; Mikkola, J.–P., Effective Dispersion of Au and Au-M (M = Co, Ni, Cu and Zn) Bimetallic Nanoparticles over TiO_2 Grafted SBA-15: Their Catalytic Activity on Dehydroisomerization of α-pinene. *Micropor. Mesopor. Mater.* **2013**, 173, 99–111.

[34] Pereira, P. H. F.; Voorwald, H. J. C.; Cioffi, M. O. H.; Da Silva, M. L. C. P.; Rego, A. M. B.; Ferraria, A. M.; De Pinho, M. N., Sugarcane Bagasse Cellulose Fibres and their Hydrous Niobium Phosphate Composites: Synthesis and Characterization by XPS, XRD and SEM. *Cellulose **2014**,* 21, 641–652.

[35] Ivashchenko, N. A.; Gac, W.; Tertykh, V. A.; Yanishpolskii, V. V.; Khainakov, S. A.; Dikhtiarenko, A. V.; Pasieczna-Patkowska, S.; Zawadzki, W., Preparation, Characterization and Catalytic Activity of Palladium Nanoparticles Embedded in the Mesoporous Silica Matrices. *World J. Nano Sci. Eng.* **2012,** 2, 117–125.

[36] Armaroli, T.; Busca, G.; Carlini, C.; Giuttarim M.; Galletti, A. M. R.; Sbrana, G., Acid Sites Characterization of Niobium Phosphate Catalysts and their Activity in Fructose Dehydration to 5-Hydroxymethyl-2-furaldehyde. *J. Mol. Catal. A: Chem.* **2000,** 151, 233–243.

[37] Bassan, I. A. L.; Nascimento, D. R.; San Gil, R. A. S.; Pais da Silva, M. I.; Moreia, C. R.; Gonzalez, W. A.; Faro Jr, A. C.; Onfroy, T.; Lachter, E. R., Esterification of Fatty Acids with Alcohols over Niobium Phosphate. *Fuel Process. Technol.* **2013,** 106, 619–624.

[38] Clayden, N. J.; Accardo, G.; Mazzei, P.; Piccolo, A.; Pernice, P.; Vergara, A.; Ferone, C.; Aronne, A., Phosphorus Stably Bonded to a Silica Gel Matrix Through Niobium Bridges. *Mater. Chem. A,* **2015,** 3, 15986–15995.

[39] Sarkar, A.; Pramanik, P., Synthesis of Mesoporous Niobium Oxophosphate using Niobium Tartrate Precursor by Soft Templating Method. *Micropor. Mesopor. Mater.,* **2009,** 117, 580–585.

[40] Jehng, J.-M.; Wachs, I. E., The Molecular Structures and Reactivity of Supported Niobium Oxide Catalysts. *Catal. Today,* **1990,** 8, 37–55.

[41] Jehng, J.-M.; Wachs, I. E., Molecular Structures of Supported Niobium Oxide Catalysts Under Ambient Conditions. *J. Mol. Catal.* **1991,** 67, 369–387.

[42] Antonettia, C.; Mellonic, M.; Licursia, D.; Fulignatia, S.; Ribechinia, E.; Rivasd, S.; Parajód, J. C.; Cavanic, F.; Gallettia, A. M. R., Microwave-assisted Dehydration of Fructose and Inulin to HMF Catalyzed by Niobium and Zirconium Phosphate Catalysts. *Appl. Catal. B: Environ.* **2017,** 206, 364–377.

[43] Lee, S. L.; Nur, H.; Hamdan, H., Physical Properties and Bifunctional Catalytic Performance of Phosphate–Vanadium Impregnated Silica–Titania Aerogel. *Catal. Lett.* **2009,** 132, 28–33.

[44] Ekhsan, J. M.; Lee, S. L.; Nur, H., Niobium Oxide and Phosphoric Acid Impregnated Silica–Titania as Oxidative-Acidic Bifunctional Catalyst. *Appl. Catal. A: Gen.* **2014,** 471, 1142–148.

[45] Konwar, L. J.; Samikannu, A.; Mäki-Arvela, P.; Mikkola, J-P., Efficient C–C coupling of bio-based furanics and carbonyl compounds to liquid hydrocarbon precursors over lignosulfonate derived acidic carbocatalysts. *Catal. Sci. Technol.* **2018**, 8, 2449–2459

Field Code Changed
Field Code Changed
Field Code Changed
Field Code Changed
Formatted: English (United States)
Formatted: English (United States)

Tables:

Table 1. Physico-chemical characterization of the catalysts

Catalysts	XRD		BET-N_2 Sorption				TPD	Total Nb and P wt.% (at.%)	
	d_{100} (nm)	Unit cell-a_0[a] (nm)	Surface area (m^2/g)	Pore diameter BJH_{Ads} (nm)	Pore Volume BJH_{Ads} (cc/g)	Pore wall thickness[b] (Å)	Total acidity (µmol/g)	Nb	P
Si-SBA-15	8.4	9.70	950.3	6.79	1.60	2.91	17	-	-
NbP-A/SBA-15	7.85	9.06	685.6	5.26	0.90	3.80	199	7.4 (1.86)	2.77 (1.66)
NbP-B/SBA-15	7.84	9.05	681.3	5.75	0.99	3.30	233	9.23 (2.06)	1.29 (0.87)
NbP-C/SBA-15 (10%)-fresh	7.81	9.02	567.3	6.88	0.99	2.14	131	7.45 (1.65)	2.43 (1.62)
NbP-C/SBA-15 (10%)-Spent	-	-	584.6	6.99	1.07	-	129	7.66 (1.78)	2.11 (1.47)
NbP-D/SBA-15	8.2	9.47	695.4	5.48	0.96	3.99	167	7.98 (1.89)	2.69 (1.82)
NbP-C/SBA-15 (5%)	7.84	9.05	570.6	6.91	0.97	2.14	69	5.02 (1.14)	1.30 (0.88)
NbP-C/SBA-15 (20%)	7.67	8.86	411.9	7.29	0.74	1.57	163	16.68 (4.11)	5.47 (4.06)
ZSM-5 (Si/Al =11.5)	-	-	-	-	-	-	1352	-	-
10%Nb_2O_5/SBA-15	-	-	571.67	5.6	0.80	-	236	-	-
NbP-bulk	-	-	131.86	4.09	0.14	-	0.276	44 (13.4)	13.1 (14.4)

[a] Unit cell parameter $a_0 = 2d_{100}/\sqrt{3}$;

[b]Pore wall thickness was calculated as: a_0 – pore diameter

Table 2. Activity of different catalyst upon conversion of butanal over different catalysts.

Catalysts	Carbonyl conversion (%) at 15 min	Carbonyl conversion (%) at 5h	HAA selectivity (%) at 5h	Turn over frequency (h^{-1})
Al-SBA-15	9.6	26	89.5	544.7
NbP-A/SBA-15	35.1	85.5	97.2	434.4
NbP-B/SBA-15	44.8	87.2	97.4	510.1
NbP-C/SBA-15 (10%)	47.5	99.6	93	982.7
NbP-D/SBA-15	32	98.8	95.1	462.3
NbP-C/SBA-15 (5%)	28.9	72.6	92.9	972
NbP-C/SBA-15 (20%)	53.2	98.3	93.6	930.4
NbP-bulk	42.2	100	97	396.7
Nb_2O_5/SBA-15	17.7	49.8	91.2	165.8
ZSM-5	11.6	16.4	84.2	18.3
No Catalyst	0	2	0	-

Reaction conditions: 50 mg catalyst, 50 ºC, 5.63 mmol 2-methylfuran, 2.5 mmol butanal, 300rpm stirring rate and no solvent.

Table 3. Activity of NbP-C/SBA-15 catalyst over the hydroxyalkylation/alkylation of different carbonyl compounds with 2methyl furan.

S.N	Reactants	HAA product	Reaction time (h)	Carbonyl conversion (%)	HAA selectivity (%)	TOF (h^{-1})
1	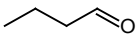	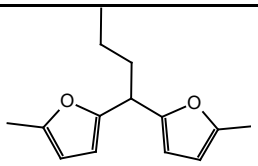	5	100	93.5	982.7
2	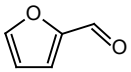	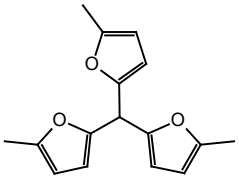	5	79.8	81.4	863.6
3	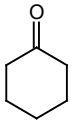	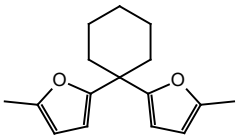	24	96.6	91.5	58.6
4		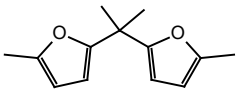	24	79.1	82.1	35.9

Reaction conditions: 50 mg catalyst, 60 ºC, 5.63 mmol 2-methylfuran, 2.5 mmol carbonyl, 300rpm stirring rate and no solvent.

Table 4. Effect of different Pd loaded catalysts upon hydrodeoxygenation of HAA products

S.N	Catalyst	HAA	Time (h)	Temp (°C)	HAA conversion (%)	HAA-hydrocarbon selectivity (%)	Total hydrocarbon selectivity (%)	Oxygenates (%)
1	Pd/NbP-A/SBA-15	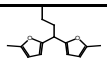	12	200	100	52.6	77.9	20.1
			12	250	100	53.1	100	0
2	Pd/NbP-B/SBA-15	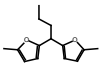	4	200	100	23.3	27.7	72.3
			8	200	100	67	94.1	5.9
			12	200	100	56.4	100	0
3	Pd/NbP-C/SBA-15 (10%)	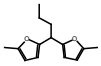	12	200	100	48.4	100	0
4	Pd/NbP-C/SBA-15 (5%)	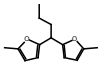	12	200	100	22.8	27.7	72.3
			12	250	100	27.6	66.2	33.8
5	Pd/NbP-C/SBA-15 (20%)	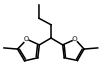	12	200	100	37.1	100	0
6	Pd/NbP-bulk	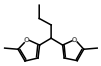	12	200	100	26.3	100	0
7	Pd/Nb_2O_5/SBA-15	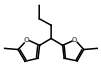	12	200	100	30.4	44.7	55.3
8	Pd/Carbon	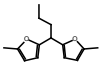	12	200	100	0	0	100
			12	300	100	52.3	100	0
9	Pd/NbP-B/SBA-15	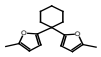	12	200	100	31.5	100	0
10	Pd/NbP-B/SBA-15	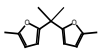	12	200	100	36.2	100	0
11	Pd/NbP-B/SBA-15	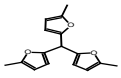	12	200	100	24.1	89.1	10.9

Reaction conditions: 100 mg catalyst, 2.5mmol HAA products, 3 mL cyclohexane solvent, 50bar H_2.

Figures:

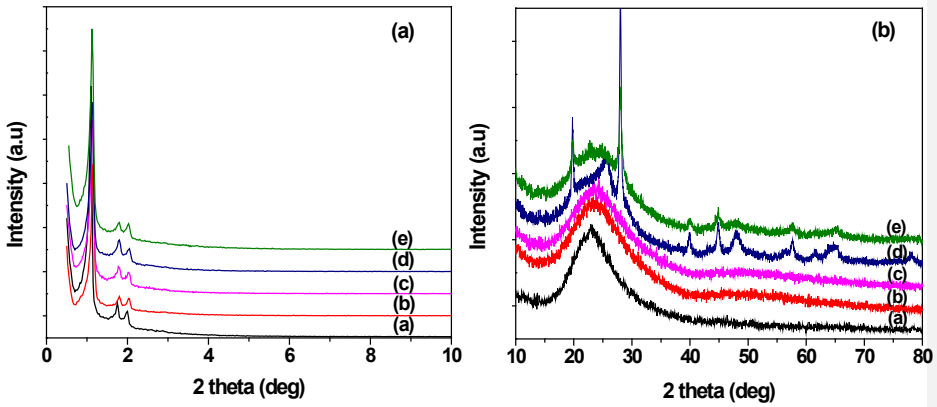

Figure 1. XRD pattern of SBA-15 supported niobium oxyphosphate catalysts prepared by different synthesis conditions: a) Low angle and b) High angle XRD pattern of (a) Si-SBA-15, (b) NbP-A/SBA-15, (c) NbP-B/SBA-15, (d) NbP-C/SBA-15, (e) NbP-D/SBA-15.

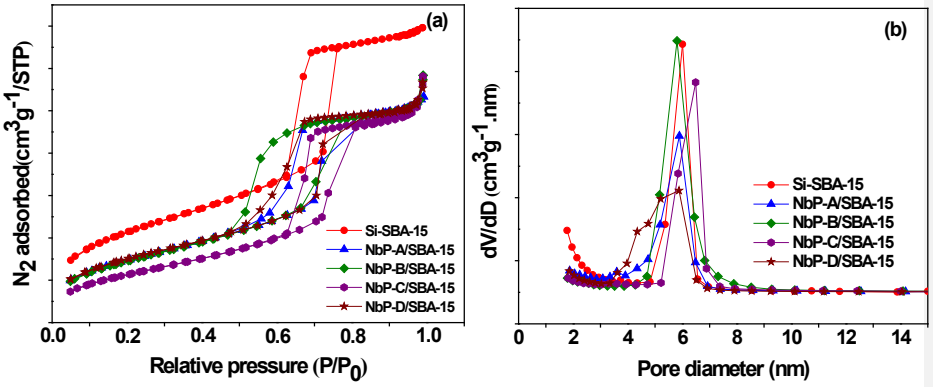

Figure 2. BET results of SBA-15 supported niobium oxyphosphate catalysts: a) N_2 adsorption-desorption isotherm and b) pore size distribution curves.

Formatted: English (United States)

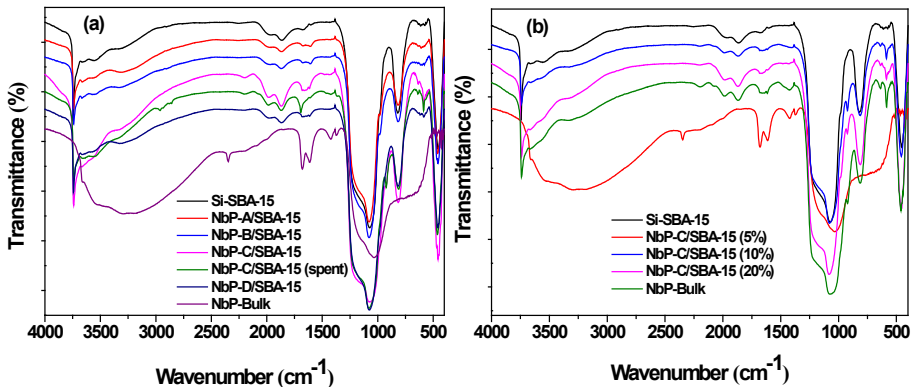

Figure 3. FT-IR spectra of SBA-15 supported niobium oxyphosphate catalysts: (a) Prepared by different synthesis conditions and (b) Different amount of niobium oxyphosphate loading on SBA-15 material.

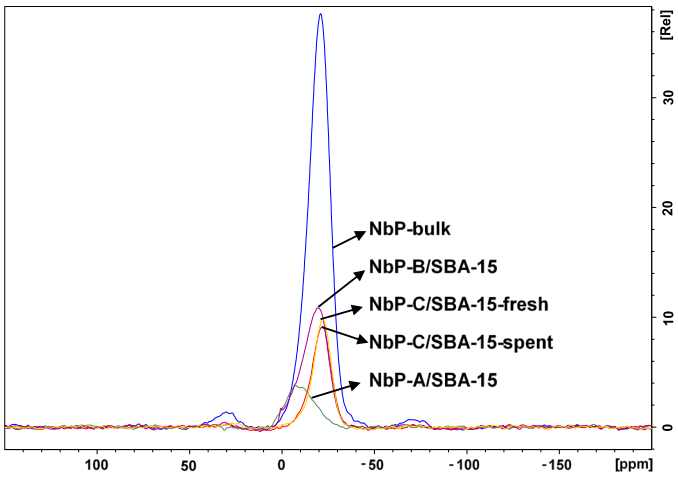

Figure 4. ^{31}P-MAS-NMR spectra of NbP supported SBA-15 catalysts.

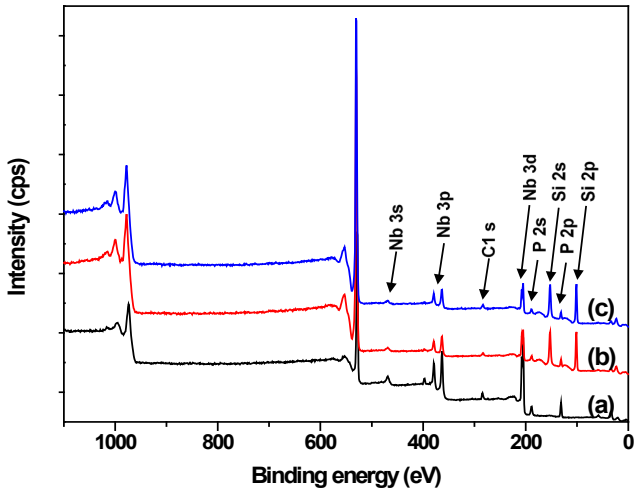

Figure 5. XPS spectra of (a)NbP-bulk (b) NbP-C/SBA-15-fresh, (c) NbP-C/SBA-15-spent catalysts.

Formatted: English (United States)

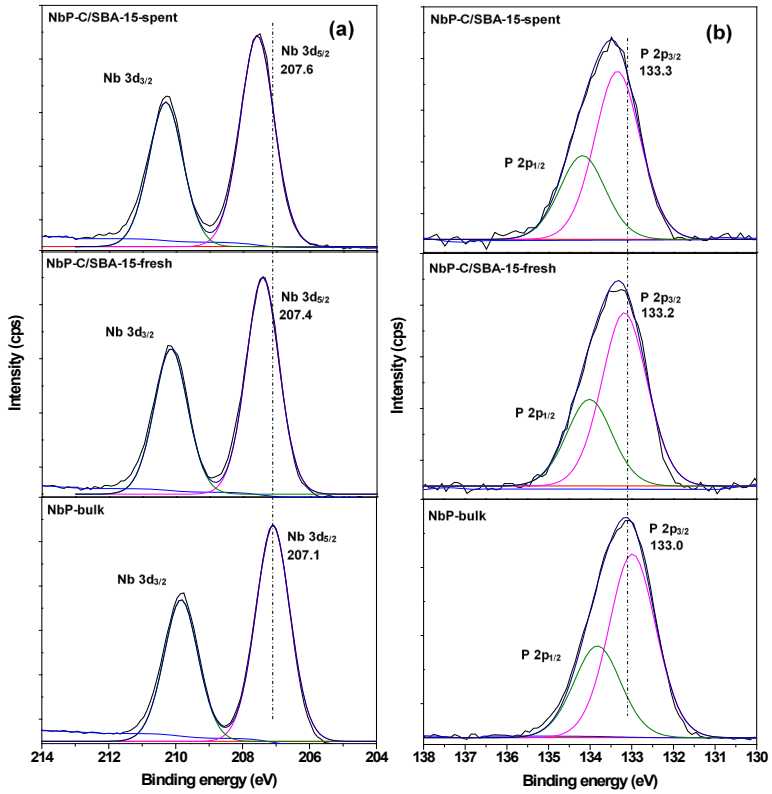

Figure 6. XPS-deconvoluted Nb3d and P2p curves for (a)NbP-bulk (b) NbP-C/SBA-15-fresh, (c) NbP-C/SBA-15-spent catalysts.

Formatted: English (United States)

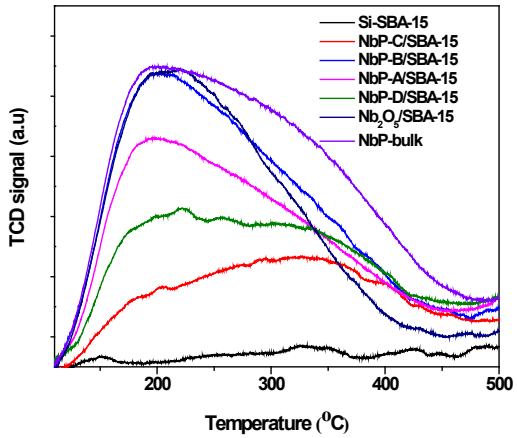

Figure 7. TPD profile of different catalysts prepared at different synthesis conditions.

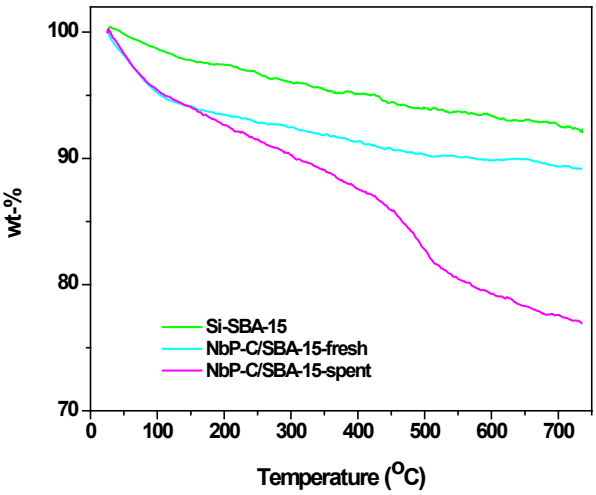

Figure 8. TGA pattern of the support and the supported NbP-C/SBA-15 catalysts.

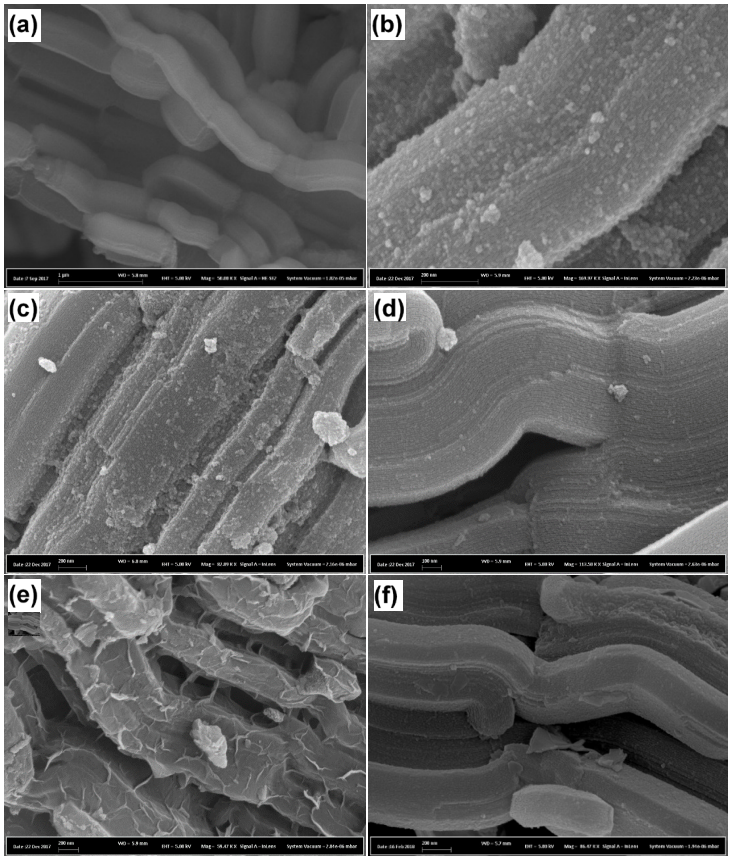

Figure 9. SEM images of (a) Si-SBA-15, (b) NbP-A/SBA-15 (c) NbP-B/SBA-15, (d) NbP-C/SBA-15, (e) NbP-D/SBA-15, (f) NbP-C/SBA-15-spent catalysts.

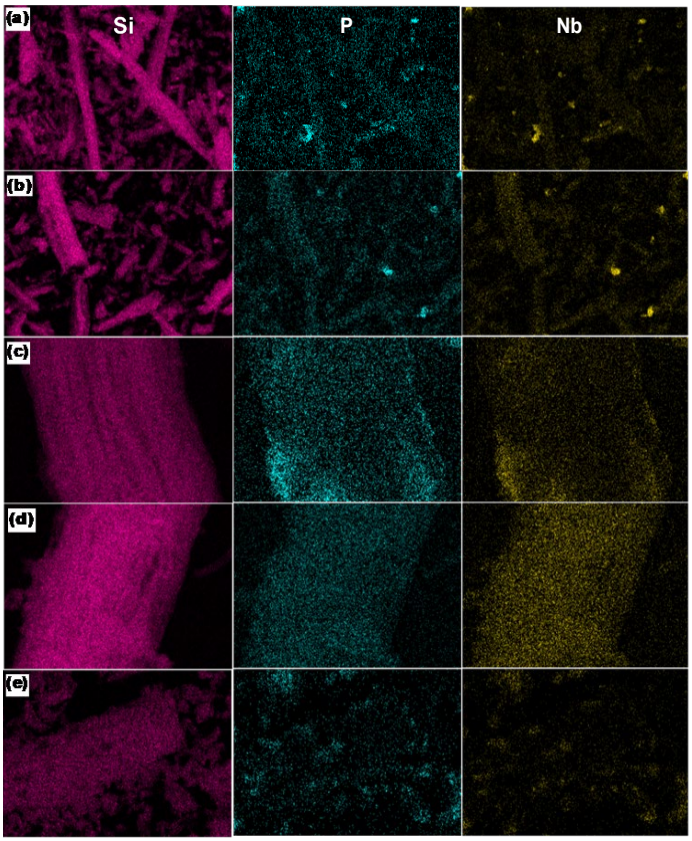

Figure 10. SEM-EDX images of (a) NbP-A/SBA-15 (b) NbP-B/SBA-15, (c) NbP-C/SBA-15, (d) NbP-D/SBA-15, (e) NbP-C/SBA-15-spent catalysts.

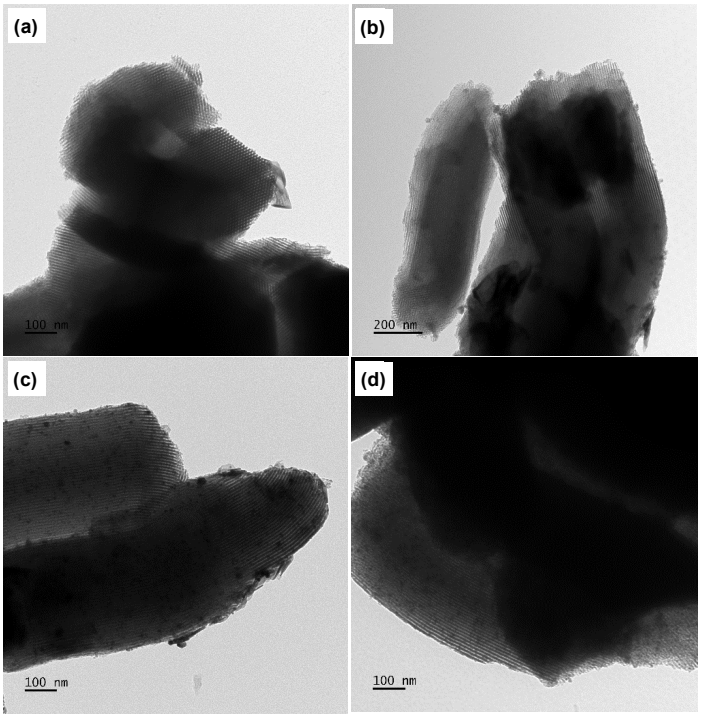

Figure 11. TEM images of (a) Si-SBA-15 (b) NbP-C/SBA-15, (c) 5%Pd/NbP-C/SBA-15, (d) NbP-B/SBA-15 catalysts.

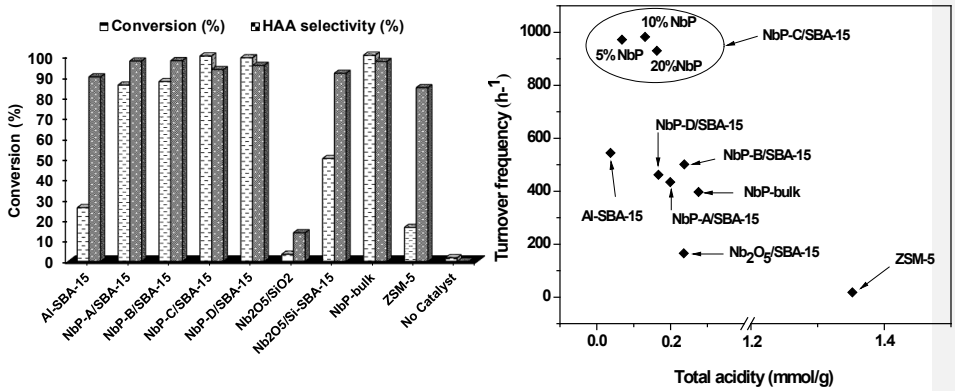

Figure 12. (a) The catalytic activity of different catalysts upon BtCHO conversion and HAA selectivity, (b) Correlation of acidity vs. TOF plot.

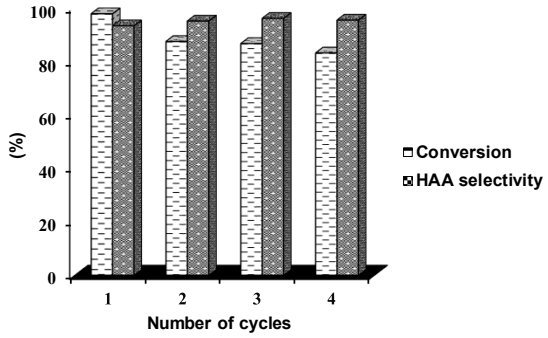

Figure 13. Reusability study of NbP-C/SBA-15 catalyst over BtCHO conversion and HAA product selectivity.

Formatted: English (United States)